

Consistent Energy-based Atomistic/Continuum Coupling for Two-body Potentials in Three Dimensions*

Alexander V. Shapeev[†]

August 16, 2011

Abstract

Very few works exist to date on development of a consistent energy-based coupling of atomistic and continuum models of materials in more than one dimension. The difficulty in constructing such a coupling consists in defining a coupled energy whose minimizers are free from uncontrollable errors on the atomistic/continuum interface. In this paper a consistent coupling in three dimensions is proposed. The main challenge in three dimensions was to identify and efficiently treat the modified Cauchy-Born continuum model which can be coupled to the exact atomistic model. The convergence and stability of the method is confirmed with numerical tests.

Keywords: Consistent energy-based atomistic/continuum coupling, quasicontinuum method, multiscale method, three dimensions

AMS subject classification: 65N30, 70C20, 74G15, 74G65

1 Introduction

Modeling defects in crystalline solids requires using atomistic models. On the one hand, defects create long-range elastic fields, accurate resolution of which requires a huge number of atomistic degrees of freedom, often unhandlable even on modern computers. On the other hand, the elastic deformation far away from a defect is well described by a continuum model. This is a rationale for *atomistic/continuum* (A/C) coupled methods—the methods that use full atomistic resolution around a defect, coupled to a coarse-grained continuum model far from the defect [10, 11, 18].

Consider a problem of finding an equilibrium of a certain atomistic crystal with a localized defect, i.e., finding a critical point of a potential energy of such a crystal. An A/C coupling approach to this problem would be to consider the exact energies of the atomistic deformation near the defect and a Cauchy-Born continuum energy of a P_1 finite element discretization of the deformation field far from the defect. The efficiency of an A/C coupling rests on the fact that the complexity of computing the energy and the effective forces associated with an element is independent of the size of the element (which would not be true if the full atomistic model was used everywhere).

*The work was performed during the author's stay at the Chair of Computational Mathematics and Numerical Analysis (ANMC) at the Swiss Federal Institute of Technology (EPFL) whose support is acknowledged.

[†]Section of Mathematics, Swiss Federal Institute of Technology (EPFL), Station 8, CH-1015, Lausanne, Switzerland (alexander@shapeev.com).

The two main variants of an A/C coupling are the energy-based and the force-based coupling, the first one defines an A/C coupled energy that depends on the atomistic and continuum deformation, while the second one mixes the atomistic and the continuum forces (i.e., derivatives of the energy of the atomistic model and the continuum model); see [11, 16, 18] and references therein for more details. The force-based coupling can indeed approximate effectively the exact atomistic equilibrium equations, however its stability properties are not well understood at present [1, 2, 11] and indeed there seem to exist examples of a force-based coupling of stable atomistic and continuum equations being unstable [15].

When using energy-based methods, one faces a different kind of challenge: it turns out to be difficult to design a coupling which is at least first order consistent (a first order consistency is equivalent to a first-order convergence provided stability)¹. Despite the recent progress in designing a consistent energy-based A/C coupling [3, 7, 14, 16, 17], no satisfactory solution exists in the general case to date.

One of the recent developments is the work [16], where the author proposed a consistent A/C coupling for two-body interaction in two dimensions. The key instrument in constructing a consistent coupling of [16] was the two-dimensional *bond density lemma*, which asserts that the effective number of atomistic bonds in a certain direction $r \in \mathbb{Z}^2$ lying on any triangle with vertices restricted to the lattice \mathbb{Z}^2 equals to the area of the triangle, regardless of the direction r . This lemma allows to define the A/C coupling method in terms of the energy of individual bonds and show that continuum approximations of bond energies sum up to a (discretized) Cauchy-Born energy, up to some correction near the interface.

The purpose of this paper is to extend the method of [16] to the three-dimensional case. Unfortunately, the three-dimensional analog of the bond-density lemma is not true: the number of bonds lying in a tetrahedron depends on the bond direction and in general is not equal to the volume of the tetrahedron. This makes the extension to 3D not trivial.

The construction of the method in 3D is similar to the lower dimensional construction: we first define the continuum energy of bonds consistent with the exact energy of the bonds, and then show that the sum of continuum energies of bonds can be computed efficiently. The resulting three-dimensional continuum model turns out to be different from the Cauchy-Born model (this is a consequence of lack of the 3D bond density lemma). Nonetheless, numerical tests conducted confirm a similar behavior as the in 2D [13, 16].

The paper is organized as follow. We formulate the proposed A/C coupling in Section 2 and define the effective number of bonds within a tetrahedron, $\text{BondVol}(T, r)$; efficient computation of this quantity is central to the overall efficiency of the proposed method. Section 3 is entirely dedicated to an efficient algorithm of computing $\text{BondVol}(T, r)$ and a Matlab code of this algorithm is given in Appendix B. In Section 4 we present numerical tests of accuracy and stability, and in Section 5 we give concluding remarks.

2 Consistent Atomistic/Continuum Coupling

For generality, we present the atomistic/continuum coupling in \mathbb{R}^d , but will mainly focus on case $d = 3$. The cases $d = 2$ (considered in [16]) and $d = 1$ (considered in [8, 16]) will be particular cases

¹in the engineering-oriented literature, a lack of consistency is formulated in terms of fictitious forces called “ghost forces”

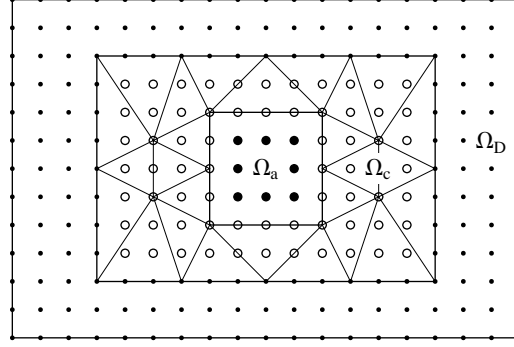


Figure 2.1: Geometry of an A/C interface. Black atoms belong to the (discrete) atomistic region Ω_a , white atoms belong to the continuum region Ω_c . The small atoms, belonging to Ω_D , are involved in posing the Dirichlet-type boundary conditions. The discrete domains are, respectively, \mathcal{L}_a , \mathcal{L}_c , and \mathcal{L}_D .

of the below discussion.

In Section 2.1 we define the continuum and discrete regions, the triangulation of the continuum region, and the corresponding functional spaces. In Section 2.2 we present an atomistic interaction in terms of bond energies. Finally, in Section 2.3 we formulate the proposed A/C coupling.

2.1 A/C Coupling Geometry

Consider an atomistic material occupying a bounded domain $\Omega \subset \mathbb{R}^d$ in its undeformed (reference) state. Assume a splitting of Ω into three (open) regions, Ω_a where the exact atomistic model will be used, Ω_c where a continuum approximation will be used, and Ω_D containing atoms whose positions will be fixed (when posing Dirichlet-type boundary conditions); see Fig. 2.1 for an illustration. The atom positions in the undeformed state comprise the lattice $\mathcal{L} = \overline{\Omega} \cap \mathbb{Z}^d$ (where \bullet denotes a closure of a set). We also denote $\mathcal{L}_D = \mathcal{L} \cap \overline{\Omega}_D$, $\mathcal{L}_c = (\mathcal{L} \cap \overline{\Omega}_c) \setminus \mathcal{L}_D$, and $\mathcal{L}_a = \mathcal{L} \setminus (\mathcal{L}_D \cup \mathcal{L}_c)$. Normally, the number of atoms in \mathcal{L}_a is much less than the total number of atoms.

It should be stressed that although we assume perfect crystalline lattices without defects in the reference configuration, the computational method can be presented if defects are allowed in the atomistic region.

We define the space of all deformations, \mathcal{U} , as all discrete functions $\mathcal{L} \rightarrow \mathbb{R}^d$ and the space of admissible displacements $\mathcal{U}_0 := \{u \in \mathcal{U} : u|_{\mathcal{L}_D} = 0\}$. Additional assumptions on \mathcal{L}_D will be made later to avoid unnecessary complications due to boundary effects.

We assume that Ω_c is a polytope (i.e., polyhedron for $d = 3$) and \mathcal{T}_h is its triangulation with simplices $T \in \mathcal{T}_h$. The spaces of A/C deformations and admissible displacements are defined as

$$\mathcal{U}^h = \{u^h : \overline{\Omega}_c \cup \mathcal{L}_a \rightarrow \mathbb{R}^d : u^h \text{ is continuous on } \Omega_c \text{ and is affine on each } T \in \mathcal{T}_h\},$$

$$\text{and } \mathcal{U}_0^h := \{u^h \in \mathcal{U}^h : u^h|_{\mathcal{L}_D} = 0\}.$$

2.2 Bond Formulation of the Atomistic Model

We assume that the atomistic interaction is given by a set of neighbors $\mathcal{R} \subset \mathbb{Z}^d \setminus \{0\}$ and a two-body potential $\phi : \mathbb{R}^d \rightarrow \mathbb{R}$. Define an interval $(x, x+r)$ between two points $x, x+r \in \mathbb{R}^2$ as a set

$$(x, x+r) := \{x + \lambda r : \lambda \in (0, 1)\}$$

and call it a *bond*; r will be called a *direction* of a bond. Introduce the finite difference associated with a bond $b = (x, x+r)$ or a bond direction r :

$$D_b y := D_r y(x) := y(x+r) - y(x),$$

and let energy of the atomistic model be

$$E(y) := \sum_{b \in \mathcal{B}} \phi(D_b y). \quad (2.1)$$

The variational equilibrium condition for $y \in \mathcal{U}$ is then

$$\langle \delta E(y), v \rangle = 0 \quad \forall v \in \mathcal{U}$$

where $\langle \bullet, \bullet \rangle$ is the scalar product in \mathcal{U} , and $\delta E(y_F) \in \mathcal{U}$ is the Gâteaux derivative of E defined as $\langle \delta E(y), v \rangle := \frac{\partial}{\partial \alpha} E(y + \alpha v) \big|_{\alpha=0}$.

We assume that $\text{dist}(\partial\Omega, \Omega \setminus \Omega_D) \geq \max_{r \in \mathcal{R}} |r|$ so that the following discrete version of the divergence theorem holds:

$$\sum_{x \in \mathcal{L} \cap (\mathcal{L} - r)} D_r v(x) = 0 \quad \forall v \in \mathcal{U}_0, \quad \forall r \in \mathcal{R}.$$

It is then easy to verify (see [16, Eq. (2.6)]) that a uniform deformation $y_F(x) := Fx$ is an equilibrium; i.e., $\langle \delta E(y_F), v \rangle = 0$.

In the next subsection we propose an A/C coupling $E^h(y)$, which is an approximation of $E(y)$, such that

$$\delta E^h(y_F) = 0; \quad (2.2)$$

in other words, $E^h(y)$ is *patch-test consistent*. This method will be a generalization of the one-dimensional method [8, 16] and the two-dimensional method [16] (more precisely, the version of the method labeled as ECC in [16]).

2.3 The Proposed A/C Coupling

Define the set of continuum bonds $\mathcal{B}_c := \{b \in \mathcal{B} : b \subset \Omega_c\}$, and the continuum directional derivative (associated with the bond direction r)

$$\nabla_r y(x) := \lim_{\epsilon \rightarrow 0} (f(x + \epsilon r) - f(x)).$$

Further, define averaging over a bond $b = (x, x+r)$:

$$\int_x^{x+r} f(x) db = \int_b f(x) db := \int_0^1 f(x + \lambda r) d\lambda.$$

The proposed (patch-test-)consistent A/C coupling then reads

$$E^h(y) := \sum_{b \in \mathcal{B}_a} \phi(D_b y) + \sum_{b \in \mathcal{B}_c} \int_b \phi(\nabla_{r_b} y) db, \quad (2.3)$$

where $\mathcal{B}_a := \mathcal{B} \setminus \mathcal{B}_c$ and r_b denotes the direction of $b \in \mathcal{B}$. The consistency (condition (2.2)) for this coupling follows from the fact that the variation of the continuum energy of a bond $b \in \mathcal{B}_c$ is equal to the variation of the exact energy on a uniform deformation y_F :

$$\langle \delta \left(\int_b \phi(\nabla_{r_b} y_F) \right) db, v \rangle = \int_b \phi(F r_b) \nabla_{r_b} v db = \phi(F r_b) D_{r_b} v = \langle \delta \phi(D_{r_b} y_F), v \rangle$$

and its proof is completely analogous to the proof of the 2D version of this statement [16, Prop. 3.2].

A straightforward calculation (see Proposition 1 below) allows us to convert bond integrals in (2.3) into a sum over elements (i.e., effectively volume integrals):

$$E^h(y) = \sum_{b \in \mathcal{B}_a} \phi(D_b y) + \sum_{T \in \mathcal{T}_h} \sum_{r \in \mathcal{R}} \Omega_{T,r} \phi(\nabla_r y|_T), \quad (2.4)$$

where the effective volumes of T are defined as

$$\Omega_{T,r} := \sum_{\substack{x \in \mathbb{Z}^d \\ (x, x+r) \in \mathcal{B}_c}} \int_x^{x+r} \chi_T db \quad (2.5)$$

and the characteristic function χ_\bullet is defined in Section 2.3.1.

It should be noted that the second term in (2.4) differs from the standard Cauchy-Born energy (for it to be equal to the Cauchy-Born energy, we must have $\Omega_{T,r} \equiv |T|$). This in particular means that the existing results on stability [4, 6] and consistency [12] of the Cauchy-Born model does not apply to the coupling proposed in the present paper. Therefore we confirm convergence and stability of the proposed coupling via numerical tests in Section 4.

2.3.1 Characteristic Function

For a polytope $\omega \subset \mathbb{R}^d$ (e.g., polyhedron in 3D) define a characteristic function

$$\chi_\omega(x) := \lim_{\rho \rightarrow 0} \frac{|\omega \cap B_\rho(x)|}{|B_\rho(x)|}, \quad (2.6)$$

where $B_\rho(x)$ is the ball centered at x with the radius ρ . We note that (i) the limit w.r.t. $\rho \rightarrow 0$ in the definition of $\chi_\omega(x)$ exists, and (ii) including/excluding the boundary of a polytope ω (or any part of it) does not change the point values of $\chi_\omega(x)$. The characteristic function is defined so that if $\bar{\omega} = \bar{\omega}_1 \cup \bar{\omega}_2$ and $\omega_1 \cap \omega_2 = \emptyset$ then $\chi_\omega = \chi_{\omega_1} + \chi_{\omega_2}$ pointwise. In particular, we have

$$\chi_{\Omega_c}(x) = \sum_{T \in \mathcal{T}_h} \chi_T(x) \quad \text{for all } x \in \mathbb{R}^2. \quad (2.7)$$

The characteristic function of a 3D polyhedron ω can be visualized as

$$\chi_\omega(x) = \begin{cases} 1 & \text{if } x \in \text{interior of } \omega \\ \frac{1}{2} & \text{if } x \in \text{face of } \omega \\ \frac{\alpha}{2\pi} & \text{if } x \in \text{edge of } \omega \text{ with angle } \alpha \\ \frac{\beta}{4\pi} & \text{if } x \text{ is a vertex of } \omega \text{ with spherical angle } \beta \\ 0 & \text{otherwise.} \end{cases} \quad (2.8)$$

Note that the values of $\chi_\omega(x)$ at the vertices of ω will not be important for the formulation of the method.

With this definition of the characteristic function, we can prove the following proposition.

Proposition 1. *The energy (2.3) is equivalently written as (2.4).*

Proof. Indeed, the second sum in (2.3) can be transformed as

$$\begin{aligned} \sum_{b \in \mathcal{B}_c} \int_b \phi(\nabla_{r_b} y) db &= \sum_{r \in \mathcal{R}} \sum_{\substack{x \in \mathbb{Z}^d \\ (x, x+r) \subset \Omega_c}} \int_x^{x+r} \phi(\nabla_r y) db \\ &= \sum_{r \in \mathcal{R}} \sum_{\substack{x \in \mathbb{Z}^d \\ (x, x+r) \subset \Omega_c}} \int_x^{x+r} \chi_{\Omega_c} \phi(\nabla_r y) db \\ &= \sum_{r \in \mathcal{R}} \sum_{\substack{x \in \mathbb{Z}^d \\ (x, x+r) \subset \Omega_c}} \int_x^{x+r} \sum_{T \in \mathcal{T}_h} \chi_T \phi(\nabla_r y) db \\ &= \sum_{T \in \mathcal{T}_h} \sum_{r \in \mathcal{R}} \phi(\nabla_r y|_T) \sum_{\substack{x \in \mathbb{Z}^d \\ (x, x+r) \subset \Omega_c}} \int_b \chi_T db, \end{aligned}$$

where we used (2.7) and the fact that $\chi_{\Omega_c} = 1$ on any bond which lies inside Ω_c . \square

2.3.2 Complexity of Computing E^h

The method (2.3) with precomputing $\Omega_{T,r}$ directly using (2.5) may already yield a significant reduction in number of operations. Indeed, one must spend $\mathcal{O}(\#(\mathcal{B}_c))$ operations (here $\#(\bullet)$ denotes the number of elements in a set) on precomputing $\Omega_{T,r}$ only once for a given A/C geometry, and it would then take $\mathcal{O}(\#(\mathcal{B}_a)) + \mathcal{O}(\#(\mathcal{T}_h)\#(\mathcal{R}))$ operations for computing the forces or assembling the stiffness matrix corresponding to (2.3) (recall that $\#(\mathcal{B}_a) \ll \#(\mathcal{B}_c)$).

Furthermore, in the 1D case and in the 2D case with triangulation nodes coinciding with the lattice sites, the bond-density lemma yields that $\Omega_{T,r} = |T|$ if T is far enough from the a/c interface and thus $E_c(y)$ reduces to the standard Cauchy-Born energy up to an interface correction. This removes the need in the precomputation step and yields an algorithm with an optimal complexity $\mathcal{O}(\#(\mathcal{B}_a)) + \mathcal{O}(\#(\mathcal{T}_h)\#(\mathcal{R}))$.

Unfortunately, as also shown in [16], in general $\Omega_{T,r} \neq |T|$ in 3D. (Numerical calculations of $\Omega_{T,r}$ with randomly generated T and r show that $\Omega_{T,r} \neq |T|$ for most choices of T and r .) Nevertheless,

Reduction to:	#(parameters)
BondVol(T, r)	15
$\gcd(r_1, r_2, r_3) = 1$	15
$r = e_3$	12
truncated prism	9
triangle	6
trapezoid	4
right triangle	2
$S_{a,b}$	2

Table 1: List of reductions from the original problem of computing $\text{BondVol}(T, r)$ to computing $S_{a,b}$, with the number of parameters left after the reduction.

as will be shown in the present paper, one can come up with an algorithm of computing $\Omega_{T,r}$ efficiently.

To this end denote, for any polytope ω ,

$$\text{BondVol}(\omega, r) := \sum_{x \in \mathbb{R}^3} \int_x^{x+r} \chi_\omega db \quad (2.9)$$

so that $\Omega_{T,r}$ can be expressed through $\text{BondVol}(T, r)$ and the interface correction:

$$\Omega_{T,r} = \text{BondVol}(T, r) - \sum_{(x, x+r) \in \mathcal{B}_a} \int_x^{x+r} \chi_T db. \quad (2.10)$$

Here the quantity $\text{BondVol}(\omega, r)$ is an effective number (volume) of all the bonds with direction r that intersect a polytope ω . In the next section we will show that $\text{BondVol}(T, r)$ can be computed with $\mathcal{O}(\log(\text{diam}(T)) + \log|r|)$ arithmetic operations in 3D. This implies an overall precomputation time of at most $\mathcal{O}((\#\mathcal{T}_h)(\#\mathcal{R})(\log(\text{diam}(\Omega)) + \log(\text{diam}(\mathcal{R})))$.

We expect that the precomputation time will not overly dominate the main computation time in most of applications. Indeed, the factor $\mathcal{O}(\log(\text{diam}(\Omega)) + \log(\text{diam}(\mathcal{R})))$ is essentially the maximal number of iterations of the Euclid's algorithm and is between 15 and 50 for a typical atomistic system with $\text{diam}(\mathcal{R}) \approx 5$ and $10^2 \lesssim \text{diam}(\Omega) \lesssim 10^9$. Indeed, in the numerical tests conducted in this paper, computing the volumes (the first term in (2.10)) was several times faster than doing the interface correction (the second term in (2.10)).

3 Computing $\text{BondVol}(T, r)$

This section is devoted entirely to an algorithm of fast computation of $\text{BondVol}(T, r)$ defined by (2.9). A reader who is not interested in details or justification of the algorithm can skip this section or refer to Appendix B for a Matlab code.

The algorithm is based on a series of steps, presented in Sections 3.1–3.3, that reduce the original problem of computing $\text{BondVol}(T, r)$ with 15 scalar parameters (12 to define T and 3 to define r) to an integer sum $S_{a,b}$ (cf. (3.13)) with only two parameters $a, b \in \mathbb{Z}$. The principle steps

of the algorithm are summarized in Table 1. The overall complexity of the algorithm is discussed in Section 3.4.

In this section by A, B, C, D, X, Y, Z we will denote the points in \mathbb{R}^3 , and by r, s, x, ξ we will denote vectors in \mathbb{R}^3 . The points may be identified with their radius vectors. For two points $X, Y \in \mathbb{R}^3$, we denote $\overrightarrow{XY} = Y - X$. For points and vectors, the subscripts 1, 2, and 3 will denote their coordinates and we will use the notation $X = (X_1, X_2, X_3)$. The standard basis of \mathbb{R}^3 will be denoted as e_1, e_2, e_3 . The points on the xy -plane in \mathbb{R}^3 (i.e., the plane $\{X \in \mathbb{R}^3 : X_3 = 0\}$) will be identified with the respective points in \mathbb{R}^2 .

3.1 Reductions

We start with a tetrahedron T and a vector $r = (r_1, r_2, r_3) \in \mathbb{Z}^3$, $r \neq 0$.

3.1.1 Reduction to the case $\gcd(r_1, r_2, r_3) = 1$

In this paragraph we show that

$$\text{BondVol}(T, r) = \text{BondVol}(T, r / \gcd(r_1, r_2, r_3)), \quad (3.1)$$

where $\gcd(r_1, r_2, r_3)$ is the greatest common divisor of $r_1, r_2, r_3 \in \mathbb{Z}$.

Indeed, let $r = ns$ with $n = \gcd(r_1, r_2, r_3) \in \mathbb{N}$ and $s \in \mathbb{Z}^3$. Fix $x \in \mathbb{Z}^3$ and consider a collection of points

$$\mathcal{X}_x = \{x + is : i \in \mathbb{Z}\}. \quad (3.2)$$

First, compute the contribution of a collection of the respective collection of bonds $\{(\xi, \xi + s) : \xi \in \mathcal{X}_x\}$ to $\text{BondVol}(T, s)$:

$$\sum_{\xi \in \mathcal{X}_x} \int_{\xi}^{\xi+s} \chi_T \text{db} = \sum_{i \in \mathbb{Z}} \int_{x+is}^{x+is+s} \chi_T \text{db} = \sum_{i \in \mathbb{Z}} \int_0^1 \chi_T(x + (i + \lambda)s) \text{d}\lambda = \int_{-\infty}^{\infty} \chi_T(x + \lambda s) \text{d}\lambda. \quad (3.3)$$

Second, compute the contributions of

$$\begin{aligned} \{(\xi, \xi + r) : \xi \in \mathcal{X}_x\} &= \{(x + is, x + is + r) : i \in \mathbb{Z}\} \\ &= \{(x + js + ir, x + js + ir + r) : i \in \mathbb{Z}, j = 0, 1, \dots, n-1\} \end{aligned}$$

to $\text{BondVol}(T, r)$:

$$\begin{aligned} \sum_{\xi \in \mathcal{X}_x} \int_{\xi}^{\xi+r} \chi_T \text{db} &= \sum_{j=0}^{n-1} \sum_{i \in \mathbb{Z}} \int_{x+js+ir}^{x+js+ir+r} \chi_T \text{db} \\ &= \sum_{j=0}^{n-1} \int_{-\infty}^{\infty} \chi_T(x + js + \lambda r) \text{d}\lambda \\ &= \frac{1}{n} \sum_{j=0}^{n-1} \int_{-\infty}^{\infty} \chi_T(x + \mu s) \text{d}\mu \\ &= \int_{-\infty}^{\infty} \chi_T(x + \mu s) \text{d}\mu, \end{aligned} \quad (3.4)$$

where we did the change of variable $\mu = j + \lambda n$.

From calculations (3.3) and (3.4) it is easy to see that $\text{BondVol}(T, s) = \text{BondVol}(T, r)$. Indeed, summing the contributions of different \mathcal{X}_x yields:

$$\begin{aligned} \text{BondVol}(T, s) &= \sum_{\mathcal{X}_x} \sum_{\xi \in \mathcal{X}_x} \int_{\xi}^{\xi+s} \chi_T \, \text{db} \\ &= \sum_{\mathcal{X}_x} \sum_{\xi \in \mathcal{X}_x} \int_{\xi}^{\xi+r} \chi_T \, \text{db} = \text{BondVol}(T, r), \end{aligned} \quad (3.5)$$

which proves (3.1).

3.1.2 Reduction to the case $r = e_3$

We now assume $\gcd(r_1, r_2, r_3) = 1$. In this subsection we first find a suitable linear transformation M such that $Mr = e_3$, and apply it to both T and r . We then extend the definitions of $\text{BondVol}(\omega, r)$ and χ_ω to allow measuring angles of edges and vertices in the untransformed space.

Construction of M . Due to Bézout lemma, there exist $c_{12}, d_{12}, c_3, d_3 \in \mathbb{Z}$ such that

$$r_1 c_{12} + r_2 d_{12} = \gcd(r_1, r_2), \quad \gcd(r_1, r_2) c_3 + r_3 d_3 = \gcd(\gcd(r_1, r_2), r_3) = 1.$$

Take matrix $M \in \mathbb{Z}^{3 \times 3}$ as the following product of two matrices:

$$M = \begin{pmatrix} r_3 & 0 & -\gcd(r_1, r_2) \\ 0 & 1 & 0 \\ c_3 & 0 & d_3 \end{pmatrix} \begin{pmatrix} c_{12} & d_{12} & 0 \\ -\frac{r_2}{\gcd(r_1, r_2)} & \frac{r_1}{\gcd(r_1, r_2)} & 0 \\ 0 & 0 & 1 \end{pmatrix}$$

and compute Mr :

$$\begin{aligned} &\begin{pmatrix} c_{12} & d_{12} & 0 \\ -\frac{r_2}{\gcd(r_1, r_2)} & \frac{r_1}{\gcd(r_1, r_2)} & 0 \\ 0 & 0 & 1 \end{pmatrix} \begin{pmatrix} r_1 \\ r_2 \\ r_3 \end{pmatrix} = \begin{pmatrix} \gcd(r_1, r_2) \\ 0 \\ r_3 \end{pmatrix}, \\ Mr &= \begin{pmatrix} r_3 & 0 & -\gcd(r_1, r_2) \\ 0 & 1 & 0 \\ c_3 & 0 & d_3 \end{pmatrix} \begin{pmatrix} \gcd(r_1, r_2) \\ 0 \\ r_3 \end{pmatrix} = \begin{pmatrix} 0 \\ 0 \\ 1 \end{pmatrix} = e_3. \end{aligned}$$

It is also important to notice that both M and M^{-1} have integer coefficients, the latter is due to $\det M = 1$. Hence

$$M\mathbb{Z}^3 = \mathbb{Z}^3. \quad (3.6)$$

Extension of χ_ω and $\text{BondVol}(\omega, r)$. We need to apply the transformation M to both T and r . To that end, we extend the definition of χ_ω by allowing for measuring angles of edges and vertices of ω after applying M :

$$\chi_\omega^M(x) := \chi_{M^{-1}\omega}(M^{-1}x),$$

so that $\chi_\omega(x) = \chi_{M\omega}^M(Mx)$. In case if ω is a polyhedron, χ_ω^M can be evaluated as

$$\chi_\omega^M(x) = \begin{cases} 1 & \text{if } x \in \text{interior of } \omega \\ \frac{1}{2} & \text{if } x \in \text{face of } \omega \\ \frac{\alpha}{2\pi} & \text{if } x \in e, e \text{ is an edge of } \omega, \alpha \text{ is the angle of } M^{-1}e \text{ in } M^{-1}\omega \\ \frac{\beta}{4\pi} & \text{if } x \text{ is a vertex of } \omega, \beta \text{ is the spherical angle of } M^{-1}x \text{ in } M^{-1}\omega \\ 0 & \text{otherwise.} \end{cases}$$

Likewise, extend

$$\text{BondVol}(M, \omega, r) := \text{BondVol}(M^{-1}\omega, M^{-1}r) = \sum_{x \in M\mathbb{Z}^3} \int_x^{x+r} \chi_\omega^M db = \sum_{x \in \mathbb{Z}^3} \int_x^{x+r} \chi_\omega^M db, \quad (3.7)$$

so that $\text{BondVol}(\omega, r) = \text{BondVol}(M, M\omega, Mr)$. Notice that in the last step of (3.7) we used (3.6). The quantity $\text{BondVol}(M, \omega, r)$ differs from $\text{BondVol}(\omega, r)$ only if r is parallel to some edge of ω and the difference is only that the angles of such edges are computed after the transformation M^{-1} is applied to them.

Thus, we reduced

$$\text{BondVol}(T, r) = \text{BondVol}(M, MT, Mr) = \text{BondVol}(M, MT, e_3).$$

3.1.3 Reduction to Truncated Prism

Denote the vertices of T by A, B, C , and D ; and choose their ordering to have a positive orientation in 3D: i.e., so that the vectors $\overrightarrow{AB}, \overrightarrow{AC}$, and \overrightarrow{AD} form a positively orientated basis.

The tetrahedron T can be represented as an oriented sum of truncated prisms, which can be rigorously expressed with characteristic functions:

$$\chi_T = -o(B'C'D')\chi_{P(BCD)} + o(A'C'D')\chi_{P(ACD)} - o(A'B'D')\chi_{P(ABD)} + o(A'B'C')\chi_{P(ABC)}, \quad (3.8)$$

where by \bullet' we denote a projection of a point or a vector on the xy -plane (i.e., on the plane orthogonal to e_3), $P(XYZ)$ is a truncated prism with vertices X, Y and Z and their projections X', Y', Z' (see Fig. 3.1 for an illustration), and $o(XYZ) \in \{-1, 0, 1\}$ is an orientation of three points $X, Y, Z \in \mathbb{Z}^2$ defined to be zero if X, Y, Z lie on the same line and to be equal to the orientation of the basis $\overrightarrow{XY}, \overrightarrow{XZ}$ otherwise.

The lower-dimensional version of (3.8) (i.e., splitting of a triangle into trapezia) is illustrated in Fig. 2(a), and the proof for an arbitrary dimension is given in Appendix A.

For convenience, we assume that all four points, A, B, C , and D , lie above the xy -plane (otherwise some prisms may be ill-defined). One, obviously, can always shift T upwards to satisfy this requirement. This, however, is not required with an appropriate generalization of $\chi_{P(XYZ)}$ when T is not entirely above the xy -plane; refer to Appendix A for more details.

Thus, we reduced computing $\text{BondVol}(T, r)$ for a tetrahedron T to computing

$$\begin{aligned} \text{BondVol}(M, T, r) = & -o(B'C'D')\text{BondVol}(M, P(BCD), r) \\ & + o(A'C'D')\text{BondVol}(M, P(ACD), r) \\ & - o(A'B'D')\text{BondVol}(M, P(ABD), r) \\ & + o(A'B'C')\text{BondVol}(M, P(ABC), r). \end{aligned}$$

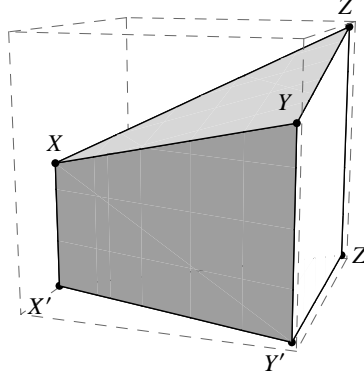


Figure 3.1: A truncated prism $P(XYZ)$ formed by three vertices X, Y, Z and their projections, X', Y' and Z' , on the xy -plane.

3.1.4 Reduction to Sums over Triangles

We have $M \in \mathbb{Z}^{3 \times 3}$, $\det M = 1$, $r = e_3$, $P = P(ABC)$ is a truncated prism, the points A, B , and C are above the xy -plane; and we need to compute $\text{BondVol}(M, P, r)$. In what follows we will use the notation $\Delta(XYZ)$ for a triangle with three vertices $X, Y, Z \in \mathbb{R}^2$.

We can assume that the plane ABC is not parallel to the z axis: otherwise $P(ABC)$ is degenerate and $\text{BondVol}(M, P, r) = 0$ (since then $\chi_P^M \equiv 0$). Hence, let $z = c_1x + c_2y + c_3$ be an equation of the plane ABC .

We will split all the bonds, as we did in (3.5), into the classes $(\xi, \xi + r)$, $\xi \in \mathcal{X}_x$ (cf. (3.2)), each class defined by $x = ie_1 + je_2$, and $i, j \in \mathbb{Z}$. That is, we express

$$\text{BondVol}(P, r) = \sum_{i,j \in \mathbb{Z}} \sum_{\xi \in \mathcal{X}_{(i,j,0)}} \int_{\xi}^{\xi+r} \chi_P^M db = \sum_{i,j \in \mathbb{Z}} \int_{-\infty}^{\infty} \chi_P^M(i, j, z) dz = \sum_{i,j \in \mathbb{Z}} \int_0^{c_1i+c_2j+c_3} \chi_P^M(i, j, z) dz.$$

For x_3 between 0 and $c_1i + c_2j + c_3$, $\chi_P^M(i, j, z)$ is equal to 1, $\frac{1}{2}$, or, respectively, $\frac{\alpha}{2\pi}$, depending on whether (i, j) is in the interior of $\Delta = \Delta(A'B'C')$, on its edge, or, respectively, on its vertex. The value α is determined by the edges, v and w , sharing the respective vertex: α is equal to the angle between the plane formed by $M^{-1}v$ and $M^{-1}e_3$ and the plane formed by $M^{-1}w$ and $M^{-1}e_3$. The latter is equal to the angle between $M^{-1}v \times M^{-1}e_3$ and $M^{-1}w \times M^{-1}e_3$.

Thus, if we define, for a polygon $S \subset \mathbb{R}^2$, its characteristic function

$$\tilde{\chi}_S^M(i, j) = \begin{cases} 1 & \text{if } (i, j) \in \text{interior of } S \\ \frac{1}{2} & \text{if } (i, j) \in \text{edge of } S \\ \frac{\alpha}{2\pi} & \text{if } (i, j) \in \text{vertex of } S \text{ sharing edges } v, w, \text{ where} \\ & \alpha \text{ is the angle between } M^{-1}v \times M^{-1}e_3 \text{ and } M^{-1}w \times M^{-1}e_3, \end{cases}$$

then

$$\int_0^{c_1i+c_2j+c_3} \chi_P^M(i, j, z) dz = (c_1i + c_2j + c_3) \tilde{\chi}_{\Delta(A'B'C')}^M(i, j),$$

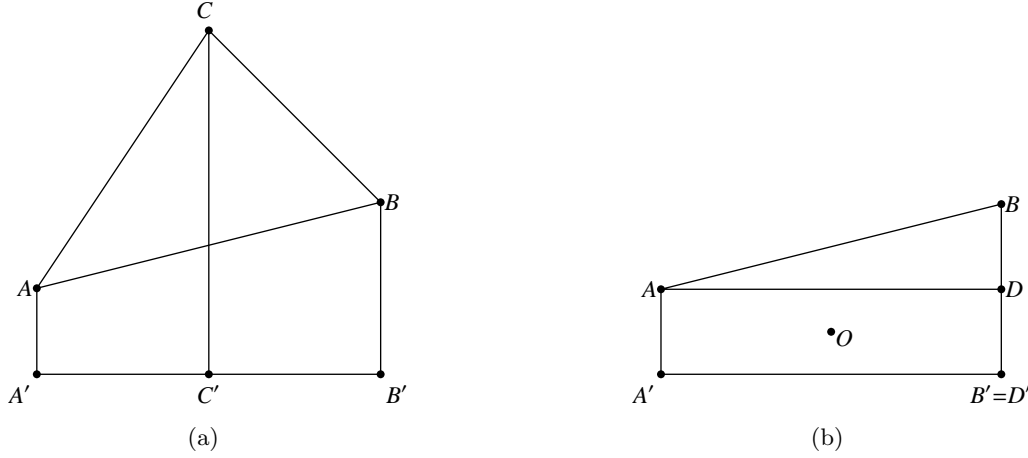


Figure 3.2: On the left: A triangle $\triangle(ABC)$ and the projections of its vertices on the x -axis. The triangle can thus be represented as an oriented sum of three trapezia, $\text{Trap}(AB)$, $\text{Trap}(BC)$, $\text{Trap}(CA)$. One can notice that the area under $\triangle(ABC)$ is counted once with minus (for $\text{Trap}(AB)$) and then with plus (for $\text{Trap}(BC)$ and $\text{Trap}(CA)$). On the right: splitting of a trapezoid $\text{Trap}(AB)$ into a right triangle $\triangle(ABD)$ and a rectangle $\text{Trap}(AD)$.

and hence

$$\begin{aligned} o(A'B'C')\text{BondVol}(P, r) &= o(A'B'C') \sum_{i,j \in \mathbb{Z}} (c_1 i + c_2 j + c_3) \tilde{\chi}_{\triangle(A'B'C')}^{\mathbf{M}}(i, j) \\ &=: S'_{A'B'C'}(\mathbf{M}; c_1, c_2, c_3). \end{aligned} \quad (3.9)$$

We thus reduced the problem to computing the sum $S'_{A'B'C'}(\mathbf{M}; c_1, c_2, c_3)$ over a triangle $\triangle(A'B'C')$.

3.1.5 Reduction to a Sum over Right Triangles

Let $\triangle = \triangle(ABC)$ and let A' , B' , and C' be the projections of A , B , C on x -axis (i.e., on e_1), as illustrated on Fig. 2(a).

Then

$$o(ABC)\tilde{\chi}_{\triangle(ABC)}^{\mathbf{M}} = -o(BC)\tilde{\chi}_{\text{Trap}(BC)}^{\mathbf{M}} + o(AC)\tilde{\chi}_{\text{Trap}(AC)}^{\mathbf{M}} - o(AB)\tilde{\chi}_{\text{Trap}(AB)}^{\mathbf{M}}, \quad (3.10)$$

where $\text{Trap}(XY)$ is a trapezoid with vertices X , Y , X' , and Y' , by \bullet' we denote a projection on the x -axis (i.e., on e_1), and $o(XY)$ is the orientation of the two points X and Y on the x -axis defined as $\text{sgn}(\overrightarrow{XY} \cdot e_1)$.

The formula (3.10) is quite intuitive: Indeed, as seen on Fig. 2(a), the area under the triangle will be counted with the minus sign when evaluating $-o(AB)\tilde{\chi}_{\text{Trap}(AB)}^{\mathbf{M}}$ and with the plus sign when evaluating $-o(BC)\tilde{\chi}_{\text{Trap}(BC)}^{\mathbf{M}} + o(AC)\tilde{\chi}_{\text{Trap}(AC)}^{\mathbf{M}}$. The proof of (3.10) is given in Appendix A.

A trapezoid $\text{Trap}(AB)$ can further be split into a right triangle and a rectangle (see an illustration on Fig. 2(b)):

$$o(AB)\tilde{\chi}_{\text{Trap}(AB)}^{\mathbf{M}} = o(ABD)\tilde{\chi}_{\triangle(ABD)}^{\mathbf{M}} + o(AD)\tilde{\chi}_{\text{Trap}(AD)}^{\mathbf{M}},$$

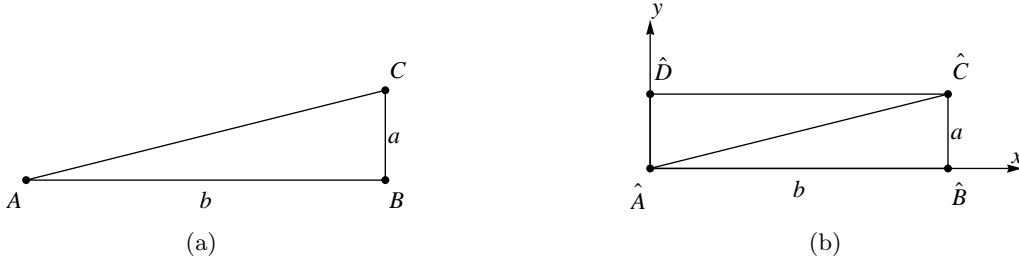


Figure 3.3: A right triangle $\triangle(ABC)$ (left) and its shifted copy $\triangle(\hat{A}\hat{B}\hat{C})$ together with its rotated copy $\triangle(\hat{C}\hat{D}\hat{A})$ (right).

where $D := (B_1, A_2)$.

Thus, we reduced our problem to two problems: (1) computing $S'_{ABC}(\mathbf{M}; c_1, c_2, c_3)$ where AB and BC are parallel to x and y axes respectively, and (2) computing

$$\sum_{i,j \in \mathbb{Z}} o(AD) \tilde{\chi}_{\text{Trap}(AD)}^{\mathbf{M}}(i, j) (c_1 i + c_2 j + c_3),$$

where AD is parallel to the x -axis. The latter can be computed analytically using the fact that the function $o(AD) \tilde{\chi}_{\text{Trap}(AD)}^{\mathbf{M}}(i, j)$ is symmetric w.r.t. rotation by the arc length π around the center O of the rectangle $\text{Trap}(AD)$:

$$\sum_{i,j \in \mathbb{Z}} o(AD) \tilde{\chi}_{\text{Trap}(AD)}^{\mathbf{M}}(i, j) (c_1 i + c_2 j + c_3) = (D_1 - A_1) A_2 (c_1 i + c_2 j + c_3) \Big|_{(i,j)=O}. \quad (3.11)$$

3.2 Computing the Sum over a Right Triangle

It remains to develop an algorithm of computing $S'_{ABC}(\mathbf{M}; c_1, c_2, c_3)$ for AB and BC parallel to x and y axes respectively, where S' is defined by (3.9).

Let $A = (A_1, A_2)$, $B = A + b e_1$, $C = B + a e_2$ (see Fig. 3(a)). We assume that both a and b are nonzero (otherwise $\triangle(ABC)$ is degenerate and $S'_{ABC}(\mathbf{M}; c_1, c_2, c_3)$ is zero).

We shift the points A , B , and C so that A coincides with the origin (see Fig. 3(b)). That is, we introduce the points $\hat{A} = (0, 0)$, $\hat{B} = (b, 0)$, $\hat{C} = (b, a)$, and change the variables of summation $i \rightarrow i - A_1$, $j \rightarrow j - A_2$:

$$\begin{aligned} S'_{ABC}(\mathbf{M}; c_1, c_2, c_3) &= o(ABC) \sum_{i,j \in \mathbb{Z}} \tilde{\chi}_{\triangle(ABC)}^{\mathbf{M}}(i + A_1, j + A_2) (c_1 i + c_2 j + c_4) \\ &=: S'_{\hat{A}\hat{B}\hat{C}}(\mathbf{M}; c_1, c_2, c_4), \end{aligned}$$

where $c_4 = c_3 + c_1 A_1 + c_2 A_2$.

Second, notice that since $\triangle(\hat{A}\hat{B}\hat{C})$ and its copy rotated by π , $\triangle(\hat{C}\hat{D}\hat{A})$ (see an illustration on Fig. 3(b)), together compose a rectangle, we can use (3.11) and express

$$S'_{\hat{A}\hat{B}\hat{C}}(\mathbf{M}; 0, 0, c_4) = \frac{1}{2} (S'_{\hat{A}\hat{B}\hat{C}}(\mathbf{M}; 0, 0, c_4) + S'_{\hat{C}\hat{D}\hat{A}}(\mathbf{M}; 0, 0, c_4)) = \frac{1}{2} ab c_4.$$

Thus, it remains to compute $S'_{\hat{A}\hat{B}\hat{C}}(\mathbf{M}; c_1, c_2, 0)$.

Third, notice that we can reduce it to the case $a, b > 0$ by doing reflections w.r.t. the axes (e.g., reflection around e_1 -axis corresponds to changing $a \rightarrow -a$, $c_1 \rightarrow -c_1$, $o(\hat{A}\hat{B}\hat{C}) \rightarrow -o(\hat{A}\hat{B}\hat{C})$). Hence we assume that $a, b > 0$ and therefore $o(\hat{A}\hat{B}\hat{C}) = o(\hat{A}\hat{B}\hat{C}) = 1$.

Last, notice that the function $\tilde{\chi}_{\Delta(\hat{A}\hat{B}\hat{C})}^{\mathbf{M}}(i, j)$ can be described as follows:

$$\tilde{\chi}_{\Delta(\hat{A}\hat{B}\hat{C})}^{\mathbf{M}}(i, j) = \begin{cases} 1 & 0 < i < b, \ 0 < j < \frac{a}{b}i \\ \frac{1}{2} & 0 < i < b, \ j = 0 \\ \frac{1}{2} & 0 < i < b, \ j = \frac{a}{b}i \\ \frac{1}{2} & i = b, \ 0 < j < a \\ \frac{\alpha}{2\pi} & i = 0, \ j = 0 \\ \frac{\beta}{2\pi} & i = b, \ j = 0 \\ \frac{\gamma}{2\pi} & i = b, \ j = a \\ 0 & \text{otherwise,} \end{cases}$$

with

$$\begin{aligned} \alpha &= \text{ang}(\mathbf{M}^{-1}(be_1) \times \mathbf{M}^{-1}e_3, \mathbf{M}^{-1}(be_1 + ae_2) \times \mathbf{M}^{-1}e_3) \\ \beta &= \text{ang}(\mathbf{M}^{-1}(be_1) \times \mathbf{M}^{-1}e_3, \mathbf{M}^{-1}(ae_2) \times \mathbf{M}^{-1}e_3) \\ \gamma &= \text{ang}(\mathbf{M}^{-1}(ae_2) \times \mathbf{M}^{-1}e_3, \mathbf{M}^{-1}(be_1 + ae_2) \times \mathbf{M}^{-1}e_3), \end{aligned}$$

where $\text{ang}(v, w) := \arccos(v \cdot w)$ for $u, v \in \mathbb{R}^3$.

Thus,

$$\begin{aligned} S'_{\hat{A}\hat{B}\hat{C}}(\mathbf{M}; c_1, c_2, 0) &= \sum_{i=1}^{b-1} \sum_{j=1}^{\lfloor \frac{ai}{b} \rfloor} (c_1 i + c_2 j) \\ &\quad - \frac{1}{2} \sum_{\substack{0 < i < b \\ i \in \gcd(a, b)\mathbb{Z}}} (c_1 i + c_2 \frac{ai}{b}) + \frac{1}{2} \sum_{j=1}^a (c_1 b + c_2 j) + \frac{1}{2} \sum_{i=1}^{b-1} (c_1 i + c_2 0) \\ &\quad + \sum_{(i, j) \in \{\hat{A}, \hat{B}, \hat{C}\}} \tilde{\chi}_{\Delta(\hat{A}\hat{B}\hat{C})}^{\mathbf{M}}(i, j). \end{aligned}$$

Each of the terms in the second line is a sum of an arithmetic progression and can be expressed analytically.

Thus, it remains to compute

$$\sum_{i=1}^{b-1} \sum_{j=1}^{\lfloor \frac{ai}{b} \rfloor} (c_1 i + c_2 j) = \sum_{i=0}^{b-1} \sum_{j=1}^{\lfloor \frac{ai}{b} \rfloor} (c_1 i + c_2 j).$$

In what follows we will use the following two standard identities that can be easily proved by induction:

$$\sum_{i=0}^{n-1} i = \frac{n(n-1)}{2}, \quad \sum_{i=0}^{n-1} i^2 = \frac{n(n-1)(2n-1)}{6}. \quad (3.12)$$

Using the second identity we can transform

$$\sum_{i=0}^{b-1} \sum_{j=1}^{\lfloor \frac{ai}{b} \rfloor} i = \sum_{i=0}^{b-1} i \left\lfloor \frac{ai}{b} \right\rfloor = \sum_{i=0}^{b-1} i \left(\frac{ai}{b} - \frac{1}{b}(ai \bmod b) \right) = \frac{1}{6}(b-1)a(2b-1) - S_{a,b},$$

where

$$S_{a,b} := \sum_{i=0}^{b-1} \frac{i}{b} (ai \bmod b); \quad (3.13)$$

and

$$\begin{aligned} \sum_{i=0}^{b-1} \sum_{j=1}^{\lfloor \frac{ai}{b} \rfloor} j &= \sum_{i=0}^{b-1} \frac{1}{2} \left\lfloor \frac{ai}{b} \right\rfloor \left(\left\lfloor \frac{ai}{b} \right\rfloor + 1 \right) \\ &= \frac{1}{2} \sum_{i=0}^{b-1} \left(\frac{ai}{b} - \frac{1}{b}(ai \bmod b) \right) \left(1 + \frac{ai}{b} - \frac{1}{b}(ai \bmod b) \right) \\ &= \frac{1}{2} \sum_{i=0}^{b-1} \frac{ai}{b} \left(1 + \frac{ai}{b} \right) - \frac{1}{2b} \sum_{i=0}^{b-1} (ai \bmod b) - \frac{1}{b} \sum_{i=0}^{b-1} \frac{ai}{b} (ai \bmod b) + \frac{1}{2b^2} \sum_{i=0}^{b-1} (ai \bmod b)^2. \end{aligned}$$

The first, second, and fourth sum can be computed analytically:

$$\sum_{i=0}^{b-1} \frac{ai}{b} \left(1 + \frac{ai}{b} \right) = \frac{a(b-1)(3b-a+2ab)}{6b}, \quad (3.14)$$

$$\sum_{i=0}^{b-1} (ai \bmod b) = \gcd(a, b) \sum_{i=0}^{\frac{b}{\gcd(a,b)}-1} \gcd(a, b) i = \frac{b(b - \gcd(a, b))}{2}, \quad (3.15)$$

$$\sum_{i=0}^{b-1} (ai \bmod b)^2 = \gcd(a, b) \sum_{i=0}^{\frac{b}{\gcd(a,b)}-1} (\gcd(a, b) i)^2 = \frac{b(b - \gcd(a, b))(2b - \gcd(a, b))}{6}, \quad (3.16)$$

and the third sum again reduces to (3.13):

$$\frac{1}{b} \sum_{i=0}^{b-1} \frac{ai}{b} (ai \bmod b) = \frac{a}{b} S_{a,b}.$$

Here the identity (3.14) follows from the standard sums (3.12); and to compute (3.15) and (3.16) we used (i) the fact that the numbers $(ai \bmod b)$, $i = 0, 1, \dots, b-1$ are essentially the numbers $\{0, \gcd(a, b), \dots, (\frac{b}{\gcd(a,b)} - 1) \gcd(a, b)\}$ repeated $\gcd(a, b)$ times each, and (ii) again the standard sums (3.12).

3.3 Computing The Sum $S_{a,b}$

For computing the sum (3.13) we propose a Euclidean-like algorithm with complexity $\mathcal{O}(\log(a+b))$, which consists in iterative reducing the (a, b) -problem to $(b \bmod a, a)$ problem.

Using the following identity [5, p. 85]:

$$\lfloor ax \rfloor = \sum_{j=0}^{a-1} \left\lfloor x + \frac{j}{a} \right\rfloor \quad \forall x \in \mathbb{R}$$

with $x = i/b$ (we assume $b \neq 0$, since $b = 0$ is a trivial case), express

$$\frac{1}{b}(ai \bmod b) = \frac{ai}{b} - \left\lfloor \frac{ai}{b} \right\rfloor = \frac{ai}{b} - \sum_{j=0}^{a-1} \left\lfloor \frac{i}{b} + \frac{j}{a} \right\rfloor.$$

Hence transform

$$S_{a,b} = \sum_{i=0}^{b-1} \frac{i}{b} (ai \bmod b) = \sum_{i=0}^{b-1} i \left(\frac{ai}{b} - \sum_{j=0}^{a-1} \left\lfloor \frac{i}{b} + \frac{j}{a} \right\rfloor \right) = \frac{a}{b} \sum_{i=0}^{b-1} i^2 - \sum_{i=0}^{b-1} \sum_{j=0}^{a-1} i \left\lfloor \frac{i}{b} + \frac{j}{a} \right\rfloor =: S_1 - S_2.$$

The first sum is trivial: $S_1 = \frac{1}{6}(b-1)a(2b-1)$.

For computing the second sum, notice that $\lfloor \frac{i}{b} + \frac{j}{a} \rfloor$ equals to 1 if $\frac{i}{b} + \frac{j}{a} \geq 1$ and 0 otherwise, and

$$\frac{i}{b} + \frac{j}{a} \geq 1 \Leftrightarrow i \geq b - \frac{bj}{a} \Leftrightarrow i \geq b - \left\lfloor \frac{bj}{a} \right\rfloor.$$

Hence

$$\begin{aligned} S_2 &= \sum_{i=0}^{b-1} \sum_{j=0}^{a-1} i \left\lfloor \frac{i}{b} + \frac{j}{a} \right\rfloor = \sum_{j=0}^{a-1} \sum_{i=b-\lfloor \frac{bj}{a} \rfloor}^{b-1} i = \sum_{j=0}^{a-1} \frac{1}{2} \left\lfloor \frac{bj}{a} \right\rfloor \left(2b-1 - \left\lfloor \frac{bj}{a} \right\rfloor \right) \\ &= \frac{1}{2} \sum_{j=0}^{a-1} \left(\frac{bj}{a} - \frac{1}{a}(bj \bmod a) \right) \left(2b-1 - \frac{bj}{a} + \frac{1}{a}(bj \bmod a) \right) \\ &= \frac{1}{2} \sum_{j=0}^{a-1} \left(\frac{b(2b-1)}{a} j - \frac{b^2}{a^2} j^2 - \frac{2b-1}{a} (bj \bmod a) + \frac{2b}{a^2} j (bj \bmod a) - \frac{1}{a^2} (bj \bmod a)^2 \right). \end{aligned}$$

We next compute individual sums in S_2 .

Using (3.15) and (3.16), evaluate the individual sums in S_2 :

$$\begin{aligned} S_2 &= \frac{1}{4}(a-1)b(2b-1) - \frac{(a-1)(2a-1)b^2}{12a} \\ &\quad + \frac{(1-2b)}{2a} \frac{(a - \gcd(a, b))a}{2} + \frac{b}{a} S_{b,a} - \frac{(a - \gcd(a, b))(2a - \gcd(a, b))}{12a}. \end{aligned}$$

Substituting this back to $S_{a,b}$ and collecting the terms yields

$$S_{a,b} = \frac{3a^2b + 3ab^2 + a^2 - 3ab + b^2 - 6ab \gcd(a, b) + \gcd(a, b)^2}{12a} - \frac{b}{a} S_{b,a}.$$

Finally, notice that $S_{b,a} = S_{b \bmod a, a}$. We thus managed to reduce the problem from (a, b) to $(b \bmod a, a)$, which yields the $\mathcal{O}(\log(a+b))$ algorithm.

3.4 Complexity of the Algorithm

Proposition 2. *The number of operations of the algorithm described in Sections 3.1–3.3 is at most $\mathcal{O}(\log(\text{diam}(T)) + \log(|r|))$.*

Proof. Evidently, $|r|$ is not increased as a result of reducing to $\gcd(r_1, r_2, r_3) = 1$ (Section 3.1.1).

In reducing to $r = e_3$ (Section 3.1.2), we can choose $0 \leq c_{12} < |r_2|$, $0 \leq d_{12} < |r_1|$, $0 \leq c_3 < |r_3|$, $0 \leq d_3 < \gcd(|r_1|, |r_2|)$. Then, up to a constant factor, $\|\mathbf{M}\|$ can be estimated as

$$\|\mathbf{M}\|_\infty \lesssim \max(|r_3| + \gcd(|r_1|, |r_2|), 1, c_3 + d_3) \max\left(c_{12} + d_{12}, \frac{|r_1| + |r_2|}{\gcd(|r_1|, |r_2|)}, 1\right) \lesssim |r|^2.$$

And hence $\text{diam}(MT) \lesssim r^2 \text{diam}(T)$.

The triangles considered in Section 3.1.4 are the bases of the truncated prisms of Section 3.1.3, which are projections of faces of MT and hence the diameter of each \triangle in Section 3.1.4 is at most $\mathcal{O}(r^2 \text{diam}(T))$. Similarly one can deduce that both a, b in each sum $S_{a,b}$ are of the order $\mathcal{O}(r^2 \text{diam}(T))$ and hence the Euclid-like algorithm of Section 3.3 takes $\mathcal{O}(\log(r^2 \text{diam}(T))) = \mathcal{O}(\log(\text{diam}(T)) + \log |r|)$ operations. \square

4 Numerical Tests

Numerical tests were conducted in order to numerically study the accuracy and stability of the method.

The atoms interact with Lennard-Jones potential $\phi(z) = -2|z|^{-6} + |z|^{-12}$ under which the FCC lattice is stable. The cut-off radius is chosen to be 3.2.

The lattice vectors are chosen as $a_1 = (0, \frac{1}{\sqrt{2}}, \frac{1}{\sqrt{2}})$, $a_2 = (\frac{1}{\sqrt{2}}, 0, \frac{1}{\sqrt{2}})$, $a_3 = (\frac{1}{\sqrt{2}}, \frac{1}{\sqrt{2}}, 0)$. The reference lattice $\mathcal{L} \setminus \mathcal{L}_D$ consists of a crystal whose atoms formed a cube with the side $2\sqrt{2}N$ ($N = 8, 16$). The Dirichlet-type boundary conditions are imposed by introducing additional atoms with fixed positions, \mathcal{L}_D . A single atom at the origin is removed thus forming a vacancy defect. In total, $\#(\mathcal{L} \setminus \mathcal{L}_D) = 125022$ (unconstrained) atoms are in the atomistic system.

A macroscopic uniform deformation with $\mathbf{F} = \begin{pmatrix} 1 & 0.01 & 0.02 \\ 0 & 1 & 0.015 \\ 0 & 0 & 1 \end{pmatrix}$ is applied to the constrained atoms \mathcal{L}_D .

The atomistic region Ω_a is chosen as a smaller cube with the side $2\sqrt{2}K$, $K = 2, 3, \dots, 11$ (see an illustration on Fig. 4.1). A quasiradial mesh with the mesh size $h = 1$ near the A/C interface is chosen in accordance with the optimal choice of meshes in 2D [13].

4.1 Accuracy Test

In the numerical tests, the exact and the approximate solutions were computed using Newton's method of solving the equilibrium equations, with the initial guess being an undeformed configuration.

The results of the computations are shown in Fig. 4.2. The difference in the $W^{1,\infty}$ -norm between the approximate and the exact deformation is plotted on the left and the difference between the energies $|E^h(u^h) - E(u)|$ is plotted on the right. One can observe at least a third order convergence in the $W^{1,\infty}$ -norm and close to fifth order convergence for the energy.

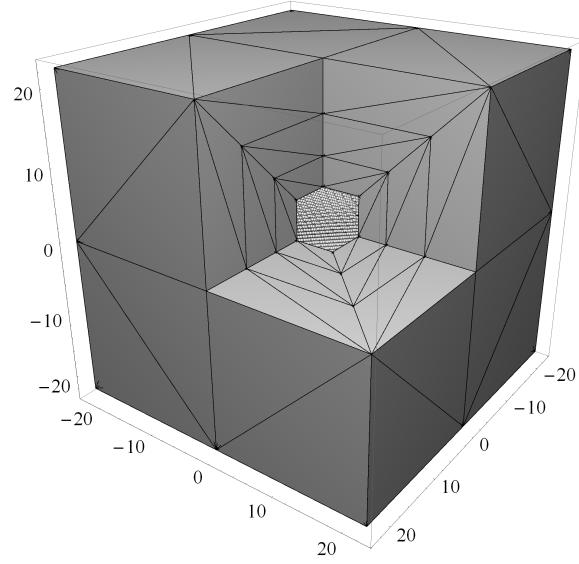


Figure 4.1: Geometry of the a/c coupling: a triangulated continuum region and atoms in the atomistic region, for $K = 2$.

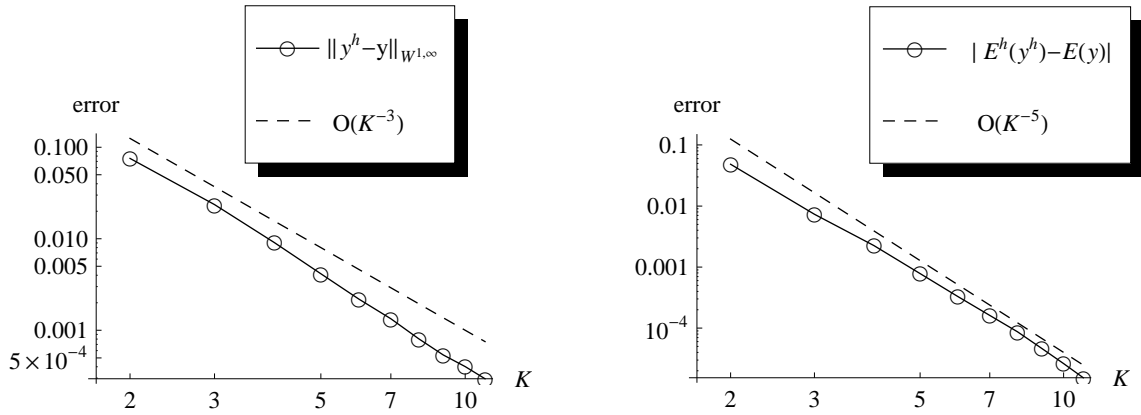


Figure 4.2: Results of computations. The $W^{1,\infty}$ -error (left) and error in energy (right) are plotted against the refinement level $K = 2, 3, \dots, 11$. One can see a third order convergence in the $W^{1,\infty}$ -norm and close to fifth order convergence for the energy.

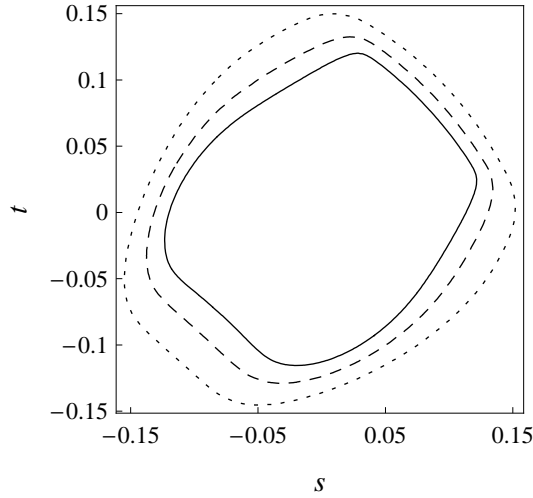


Figure 4.3: Stability regions for a Bravais lattice. The solid line corresponds to the exact stability region of the infinite lattice, the dashed line corresponds to the coupling with $N = 16$ and $K = 8$, and the dotted line corresponds to the coupling with $N = 8$ and $K = 4$. The results suggest that the coupled A/C system does not lose stability earlier than the original atomistic system.

4.2 Stability Tests for a Bravais Lattice

We also conducted stability tests for a Bravais lattice (i.e., with no defects) to verify that the stability region of the proposed coupling E^h is not smaller than the stability region of the atomistic model E . This is crucial in numerically studying defects: it must be made sure that the onset of instability occurs due to motion of a defect but not due to artifacts of the coupling.

We take a Bravais lattice $\mathcal{L} \setminus \mathcal{L}_D$ similar to the previously described but with no removed atoms. The macroscopic uniform deformation gradient $\mathbf{F} = \begin{pmatrix} 1+t & 0.05 & 0.02 \\ 0 & 1+s & 0.01 \\ 0 & 0 & 1 \end{pmatrix}$ is applied to the constrained atoms \mathcal{L}_D . The two parameters, t and s , were varied in the range between -0.2 and 0.2 .

We computed stability regions for the coupling E^h and compared it to the stability region of the exact atomistic model on an infinite lattice. A stability region is defined as the set of parameters (t, s) for which the model is stable. Stability of E^h was determined by numerically testing whether the Hessian $\delta^2 E^h$ is positive definite. The stability of the atomistic model was computed analytically with the help of Fourier transform [6].

The stability regions are plotted in Fig. 4.3. The solid line corresponds to the exact stability region of the infinite lattice, the dashed line corresponds to the coupling with $N = 16$ and $K = 8$, and the dotted line corresponds to the coupling with $N = 8$ and $K = 4$. One can see that stability regions of the coupling strictly contain the exact stability region and seem to approach it as N and K increase, which is the desired behavior of the A/C coupling.

5 Discussion and Conclusion

In the present paper the consistent A/C coupling [16] has been extended to 3D for two-body potentials. The proposed method couples the atomistic equations with the modified Cauchy-Born continuum model. The continuum energy of the modified model can be evaluated efficiently, as discussed in Section 3. Although the stability of such a modified continuum model has not been studied analytically in the existing literature, the numerical tests suggest that the proposed coupling is stable whenever the atomistic model is stable. The numerical tests also confirm convergence of the proposed coupling to the exact solution.

The major challenge yet to be solved is an extension of the present method to many-body interaction. A one-dimensional consistent coupling for such an interaction exists [9], however it does not seem obvious how to define continuum approximations to many-body bond energies in many dimensions.

Acknowledgments

The author thanks Christoph Ortner for his valuable comments and advices that led to improvement of the manuscript. The author also appreciated a discussion with Alla Merzakreeva who brought the author's attention to the existing developments in Computer Science related to integer sums.

A Splitting a Simplex into Truncated Prisms

A.1 Auxiliary Definitions

We define an orientation of points $X^{(1)}, \dots, X^{(d+1)} \in \mathbb{R}^d$ as an orientation of the basis $(X^{(2)} - X^{(1)}, \dots, X^{(d+1)} - X^{(1)})$; i.e.

$$o_d(X^{(1)}, \dots, X^{(d+1)}) := \text{sgn} \circ \det \begin{pmatrix} X_1^{(2)} - X_1^{(1)} & X_2^{(2)} - X_2^{(1)} & \dots & X_d^{(2)} - X_d^{(1)} \\ X_1^{(3)} - X_1^{(1)} & X_2^{(3)} - X_2^{(1)} & \dots & X_d^{(3)} - X_d^{(1)} \\ \vdots & \vdots & \ddots & \vdots \\ X_1^{(d+1)} - X_1^{(1)} & X_2^{(d+1)} - X_2^{(1)} & \dots & X_d^{(d+1)} - X_d^{(1)} \end{pmatrix}, \quad (\text{A.1})$$

$o_d(X^{(1)}, \dots, X^{(d+1)}) \in \{-1, 0, 1\}$.

Next, we define the characteristic function of a truncated prism $P = P(X^{(1)}, \dots, X^{(d)})$ for d points $X^{(1)}, \dots, X^{(d)} \in \mathbb{R}^d$. If the plane through these d points is perpendicular to the hyperplane $x_d = 0$ then we let $\chi_P := 0$. Otherwise let $x_d = \sum_{i=1}^{d-1} \alpha_i x_i$ be an equation of such a plane and define $\tilde{\chi}_P \in L_1(\mathbb{R}^d)$,

$$\tilde{\chi}_P := \begin{cases} 1 & 0 < x_d < \sum_{i=1}^{d-1} \alpha_i x_i \text{ and } \xi \in \text{conv}((X^{(1)})', \dots, (X^{(d)})'), \\ -1 & 0 > x_d > \sum_{i=1}^{d-1} \alpha_i x_i \text{ and } \xi \in \text{conv}((X^{(1)})', \dots, (X^{(d)})'), \\ 0 & \text{otherwise,} \end{cases} \quad (\text{A.2})$$

and

$$\chi_P(x) := \lim_{\rho \rightarrow 0} \frac{1}{|B_\rho(x)|} \int_{B_\rho(x)} \tilde{\chi}_P(\xi) d\xi, \quad (\text{A.3})$$

where by \bullet' we denote an orthogonal projection on the hyperplane $x_d = 0$.

Notice that $\chi_P = \tilde{\chi}_P$ almost everywhere (χ_P is defined pointwise in \mathbb{R}^d and may take intermediate values conforming with the definition (2.6)). Also notice that χ_P is a characteristic function of a polytope P in the sense of (2.6) only when the face $\text{conv}(X^{(1)}, \dots, X^{(d)})$ is “high enough” (i.e., has a large enough x_d -coordinate). Otherwise, writing $P = P(X^{(1)}, \dots, X^{(d)})$ is formal and does not refer to a proper polytope in \mathbb{R}^d .

A.2 Formulation of the Result

Let $A^{(1)}, \dots, A^{(d+1)} \in \mathbb{R}^d$ so that $o_d(A^{(1)}, \dots, A^{(d+1)}) = 1$. Denote

$$\begin{array}{ll} \text{the simplex} & T := \text{conv}(A^{(1)}, \dots, A^{(d+1)}), \\ \text{the truncated prisms} & P^{(k)} := P(A^{(1)}, \dots, A^{(k-1)}, A^{(k+1)}, \dots, A^{(d+1)}), \\ \text{their orientations} & o^{(k)} := o_{d-1}((A^{(1)})', \dots, (A^{(k-1)})', (A^{(k+1)})', \dots, (A^{(d+1)})'), \\ \text{and the faces of } T, & F^{(k)} = \text{conv}(A^{(1)}, \dots, A^{(k-1)}, A^{(k+1)}, \dots, A^{(d+1)}), \end{array}$$

where $k = 1, \dots, d+1$. Here we identify points on the hyperplane $x_d = 0$ with points in \mathbb{R}^{d-1} when computing orientations $o^{(k)}$ via (A.1)

We prove

Proposition 3.

$$\chi_T = - \sum_{k=1}^{d+1} (-1)^k o^{(k)} \chi_{P^{(k)}} \quad (\text{A.4})$$

pointwise in \mathbb{R}^d , where χ_T is defined by (2.6).

A.3 Proof

In the following two lemmas we prove that (A.4) holds almost everywhere.

Lemma 1. *The relation (A.4) holds almost everywhere in \mathbb{R}^d if $A_d^{(k)} \geq 0$ for all $k = 1, \dots, d+1$ (i.e., if T is entirely above the hyperplane $x_d = 0$).*

Proof. Since all vertices $A^{(k)}$ lie above the hyperplane $x_d = 0$, the function χ_P defined by (A.2) and (A.3) equals 1 or 0 almost everywhere and hence is the characteristic function of a proper truncated prism P .

Fix an arbitrary test function $f \in C^\infty(\mathbb{R}^d)$, and let

$$g(x_1, \dots, x_{d-1}, x_d) := e_d \int_0^{x_d} f(x_1, \dots, x_{d-1}, \xi) d\xi$$

so that $f = \text{div} g$ (recall that e_1, \dots, e_d is the canonical basis of \mathbb{R}^d). Multiply (A.4) by f and apply the divergence theorem:

$$\int_{\partial T} g \cdot n^T d\gamma = - \sum_{k=1}^{d+1} (-1)^k \int_{\partial P^{(k)}} o^{(k)} g \cdot n^{P^{(k)}} d\gamma, \quad (\text{A.5})$$

where n^\bullet is the outward normal vector (to T or $P^{(k)}$ respectively).

Next, notice that $g = 0$ on the base of the truncated prims (i.e., for $x_d = 0$) by the definition of g and $g \cdot n^{P^{(k)}} = 0$ on the sides of the truncated prism (i.e., below $F^{(k)}$). Hence, in both parts of the relation (A.5) we have the sum over faces $F^{(k)}$ of the integrals of $g \cdot n^\bullet$ and it only remains to verify that $n^T = -(-1)^k o^{(k)} n^{P^{(k)}}$ for all k .

To prove that, fix $k \in \{1, \dots, d+1\}$ such that $P^{(k)}$ is not degenerate (otherwise the statement is trivial since $n^{P^{(k)}} = 0$ and $n^T = 0$ on that face of T). Notice that $n_d^{P^{(k)}} > 0$ (i.e., the vector $n_{P^{(k)}}$ points upwards). The agreement of orientation of n^T and $o^{(k)}$ follows from the following chain of statements:

$$\begin{aligned} o^{(k)} &= (-1)^k \\ \Leftrightarrow o_d(A^{(1)}, \dots, A^{(k-1)}, A^{(k+1)}, \dots, A^{(d+1)}, A^{(\ell)} + e_d) &= (-1)^k \\ \Leftrightarrow o_d(A^{(1)}, \dots, A^{(k-1)}, A^{(\ell)} + e_d, A^{(k+1)}, \dots, A^{(d+1)}) &= 1 \\ \Leftrightarrow e_d \text{ is an inward vector w.r.t. } F^{(k)} \\ \Leftrightarrow n_d^T < 0, \end{aligned}$$

where ℓ is any integer between 1 and $d+1$ different from k . Here in the first step we used the expansion of determinant by minors and in the third step the following fact: Since the basis $(A^{(2)} - A^{(1)}, \dots, A^{(d+1)} - A^{(1)})$ is positively oriented, a vector v is an inward (or, resp., outward) vector w.r.t. $F^{(k)}$ if and only if the orientation of the basis $(A^{(2)} - A^{(1)}, \dots, A^{(k-1)} - A^{(1)}, v, A^{(k+1)} - A^{(1)}, \dots, A^{(d+1)} - A^{(1)})$ is positive (or, resp., negative). \square

Lemma 2. *The relation (A.4) holds almost everywhere in \mathbb{R}^d .*

Proof. In view of the previous lemma, we only need to show that both sides of (A.4) are invariant w.r.t. S_D , a dilatation in x_d by distance D . More precisely, we need to notice that $S_D \chi_T = \chi_{S_D T}$ almost everywhere (which follows directly from the definition of χ) and prove that

$$\sum_{k=1}^{d+1} (-1)^k o^{(k)} S_D \circ \chi_{P^{(k)}} = \sum_{k=1}^{d+1} (-1)^k o^{(k)} \chi_{S_D P^{(k)}}. \quad (\text{A.6})$$

Proof of (A.6) is based on noticing that

$$\chi_{S_D P(X^{(1)}, \dots, X^{(d)})} = S_D \circ \chi_{P(X^{(1)}, \dots, X^{(d)})} + \chi_{P(De_d + (X^{(1)})', \dots, (De_d + X^{(d)})')},$$

i.e., that χ of a shifted truncated prims equals to shifted χ of a truncated prism plus χ of a prism of height D with the base formed by prjections $(X^{(1)})', \dots, (X^{(d)})'$. This can be verified by fixing $x \in \text{conv}((X^{(1)})', \dots, (X^{(d)})')$ (for x elsewhere the statement is trivial) and considering three cases: $\sum_{i=1}^{d-1} \alpha_i x_i$ is (i) less than $\min(0, D)$, (ii) between $\min(0, D)$ and $\max(0, D)$, and (iii) greater than $\max(0, D)$.

We now take the difference between the left-hand side and the right-hand side of (A.6):

$$\sum_{k=1}^{d+1} (-1)^k o^{(k)} S_D \circ \chi_{P^{(k)}} - \sum_{k=1}^{d+1} (-1)^k o^{(k)} \chi_{S_D P^{(k)}} = \sum_{k=1}^{d+1} (-1)^k o^{(k)} \chi_{S_D (F^{(k)})'} \quad (\text{A.7})$$

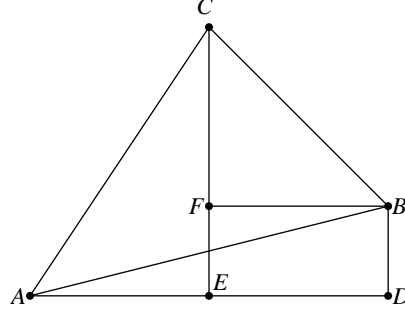


Figure B.1: An alternative splitting of $\triangle(ABC)$ into three right triangles and a rectangle.

and notice that this difference depends only on projections of faces, $(F^{(k)})'$, but not on d -th coordinate of the points $A^{(1)}, \dots, A^{(d+1)}$. Hence we can again shift these points so that Lemma 1 applies to both T and $S_D T$ and hence conclude that the difference (A.7) equals to $S_D \circ \chi_T - \chi_{S_D T} = 0$ almost everywhere. \square

We now finalize the proof of Proposition 3.

Proof of Proposition 3. Denote $f(x) = \chi_T(x) + \sum_{k=1}^{d+1} (-1)^k o^{(k)} \chi_{P^{(k)}}(x)$. From (2.6) and (A.3) we have

$$f(x) = \lim_{\rho \rightarrow 0} \frac{1}{|B_\rho(x)|} \int_{B_\rho(x)} f(\xi) d\xi. \quad (\text{A.8})$$

Due to lemma 2, $f(\xi) = 0$ for almost all ξ , hence the right-hand side of (A.8) is zero, hence $f(x) = 0$ for all $x \in \mathbb{R}^d$. \square

B A Matlab implementation of computation of $\text{BondVol}(T, r)$

The code given in this appendix closely follows the algorithm outlined in Section 3 except for the following optimization.

Instead of the splitting (3.10) we introduce three additional points $D = (B_1, A_2)$, $E = (C_1, A_2)$, $F = (C_1, B_2)$ (see Fig. B.1) and represent

$$\begin{aligned} o(ABC) \tilde{\chi}_{\triangle(ABC)}^M &= -o(ADB) \tilde{\chi}_{\triangle(ADB)}^M \\ &\quad + o(AEC) \tilde{\chi}_{\triangle(AEC)}^M \\ &\quad + o(FBC) \tilde{\chi}_{\triangle(FBC)}^M \\ &\quad + o(EDB) \tilde{\chi}_{\square(EDBF)}^M, \end{aligned}$$

where $\square(EDBF)$ is the rectangle $EDBF$. The contribution of the latter is computed by a formula analogous to (3.11).

The Matlab Code

```

function BondVol = BondVol_tetrahedron(v, r)
% BondVol(v,r) of the tetrahedron with vertices v

    % change the coordinates so that r = (0,0,1)
    [gcd12, c12, d12] = gcd(r(1),r(2));
    [gcd3, c3, d3] = gcd(gcd12,r(3));
    if(gcd3~=1)
        % reduce to the case gcd3=1
        r = r/gcd3;
        gcd12 = gcd12 /gcd3;
    end
    M = eye(3);
    if(r(1) ~=0 || r(2) ~=0 || r(3) == 0)
        M = [c12,d12,0;r(2)/gcd12, -r(1)/gcd12, 0;0,0,1];
        M = [-r(3),0,gcd12;0,1,0;c3,0,d3]*M;

        r = M*r;
        v = M*v;
    end

    invM = inv(M);
    BondVol = BondVol_prism(v(:,[1;2;3]), invM) + ...
        BondVol_prism(v(:,[4;3;2]), invM) + ...
        BondVol_prism(v(:,[4;2;1]), invM) + ...
        BondVol_prism(v(:,[1;3;4]), invM);
end

function BondVol = BondVol_prism(v, invM)
% BondVol(v,r) of the truncated prism,
% formed by three vertices v and their projections on the XY plane;
% r is assumed to be (0,0,1);
% invM*r and invM*v are the original positions.

    % shift the triangle (and the prism) so that v1 = (0,0,*)
    v([1 2],2)=v([1 2],2)-v([1 2],1);
    v([1 2],3)=v([1 2],3)-v([1 2],1);
    v([1 2],1)=[0;0];

    if(round(det([1;1;1], v([1 2],:))')==0)
        % if the prism is degenerate
        BondVol = 0;
    else
        % find coefficients [c4; c1; c2] of the function c1*i + c2*j + c4 that we sum
        c4c1c2 = [[1;1;1], v([1 2],:)]'\v(3,:);

        % reduce to integration over a triangle formed by (0,0), (v2x, v2y), (v3x, v3y),
        % which is further reduced to integration over three right triangles and
        % one rectrangle
        BondVol = + right_triangle_sum(c4c1c2, v([1 2],2), invM) ...

```



```

- right_triangle_sum(c4c1c2, v([1 2],3), invM) ...
- right_triangle_sum(c4c1c2 + ...
    [1;0;0]*([0 v([1 2],3)]*c4c1c2), v([1 2],2)-v([1 2],3), invM) ...
+ prod(v([1 2],3)-[v(1,2);0])* ([1 0.5*(v([1 2],3)+[v(1,2);0])]' * c4c1c2);

end
end

function ans = right_triangle_sum(c4c1c2, pt, invM)
% sum c4 + c1 x + c2 y over a right triangle (0,0), (pt(1),0), pt

b = pt(1); % x-side
a = pt(2); % y-side

if(a==0 || b==0)
    ans = 0; return;
end

% reduce to a>0 and b>0
orientation = sign(a)*sign(b);
c4c1c2 = c4c1c2 .* [1;sign(b);sign(a)];
invM = invM*diag([sign(b), sign(a), 1]);
a=abs(a); b=abs(b);

% sum the constant term
ans = 1/2*a*b*c4c1c2(1);
c1c2 = c4c1c2(2:3);

% sum the linear terms, using reduction to Sab
gcdab = gcd(a,b);
Sab_ans=Sab(a,b,gcdab);
ans = ans + c4c1c2(2) * (1/6*a*(b-1)*(2*b-1) - Sab_ans);
ans = ans + c4c1c2(3) * (1/4*(a-1)*(b-1) + 1/4*(gcdab-1) ...
    + 1/12*(a^2)/b*(b-1)*(2*b-1) + 1/12/b*(b-gcdab)*(2*b-gcdab) - a/b*Sab_ans);

% sum over sides:
ans = ans + 0.5*(a-1)* [b a/2]*c1c2;
ans = ans + 0.5*(b-1)* [b/2 0]*c1c2;

% sum over the hypotenuse (we subtract half the contribution)
ans = ans - 0.5*(gcdab-1)* [b/2 a/2]*c1c2;

% sum over vertices
v1 = cross(invM(:,1),invM(:,3)); % invM(:,1) == invM*[1;0;0]
v2 = cross(invM(:,2),invM(:,3));
v3 = -cross(invM*[b;a;0],invM(:,3));
i = 0; j = 0;
ans = ans + acos(dot(v1,-v3)/norm(v1)/norm(v3))/(2*pi) * [i j]*c1c2;
i = b; j = a;
ans = ans + acos(dot(-v2,v3)/norm(v2)/norm(v3))/(2*pi) * [i j]*c1c2;
i = b; j = 0;

```

```

    ans = ans + acos(dot(-v1,v2)/norm(v1)/norm(v2))/(2*pi) * [i j]*c1c2;

    ans = real(ans) * orientation;
end

function ans = Sab(a,b, gcdab)
% sums i/b (a*i mod b) over i=0..b-1

    if(b==0)
        ans=0; return;
    end

    result = 0; multiplier = 1;

    while(a ~= 0)
        result = result + multiplier * ...
            (3*b*a^2 + 3*b^2*a + a^2 - 3*a*b + b^2 - 6*a*b*gcdab + gcdab^2)/(12*a);
        multiplier = multiplier * (-b/a);
        old_b=b; b=a; a=mod(old_b,b);
    end
end

```

References

- [1] M. Dobson, M. Luskin, and C. Ortner. Sharp stability estimates for force-based quasicontinuum methods. *Multiscale Modeling & Simulation*, 8(3):782–802, 2010.
- [2] M. Dobson, M. Luskin, and C. Ortner. Stability, instability, and error of the force-based quasicontinuum approximation. *Archive for Rational Mechanics and Analysis*, 197(1):179–202, 2010.
- [3] W. E, J. Lu, and J. Z. Yang. Uniform accuracy of the quasicontinuum method. *Physical Review B*, 74(21):214115(1–12), 2006.
- [4] W. E and P. Ming. Cauchy-Born rule and the stability of crystalline solids: Static problems. *Archive for Rational Mechanics and Analysis*, 183:241–297, 2007.
- [5] R. L. Graham, D. E. Knuth, and O. Patashnik. *Concrete Mathematics*. Boston: Addison-Wesley, 2nd edition, 2004.
- [6] T. Hudson and C. Ortner. Linear stability of atomistic energies and their Cauchy–Born approximations. OxMOS Preprint No. 31/2010.
- [7] M. Iyer and V. Gavini. A field theoretic approach to the quasi-continuum method. *J. Mech. Phys. Solids*, 59:1506–1535, 2011.
- [8] X. H. Li and M. Luskin. A generalized quasinonlocal atomistic-to-continuum coupling method with finite-range interaction. *IMA J. Numer. Anal.*, to appear. arXiv:1007.2336.

- [9] Xingjie Helen Li and Mitchell Luskin. An analysis of the quasi-nonlocal quasicontinuum approximation of the embedded atom model, to appear. arXiv:1008.3628v4.
- [10] R. E. Miller and E. B. Tadmor. The quasicontinuum method: Overview, applications and current directions. *Journal of Computer-Aided Materials Design*, 9:203–239, 2002.
- [11] R. E. Miller and E. B. Tadmor. A unified framework and performance benchmark of fourteen multiscale atomistic/continuum coupling methods. *Modelling and Simulation In Materials Science and Engineering*, 17(5):053001, 2009.
- [12] C. Ortner. The role of the patch test in 2D atomistic-to-continuum coupling methods. arXiv:1101.5256v2.
- [13] C. Ortner and A. V. Shapeev. Analysis of an energy-based atomistic/continuum coupling approximation of a vacancy in the 2D triangular lattice. arXiv:1104.0311.
- [14] C. Ortner and L. Zhang. manuscript.
- [15] A. V. Shapeev. In preparation.
- [16] A. V. Shapeev. Consistent energy-based atomistic/continuum coupling for two-body potentials in one and two dimensions. *Multiscale Model. Simul.*, 9(3):905–932, 2011.
- [17] T. Shimokawa, J. J. Mortensen, J. Schiøtz, and K. W. Jacobsen. Matching conditions in the quasicontinuum method: Removal of the error introduced at the interface between the coarse-grained and fully atomistic region. *Physical Review B*, 69:214104(1–10), 2004.
- [18] B. Van Koten, X. H. Li, M. Luskin, and C. Ortner. A computational and theoretical investigation of the accuracy of quasicontinuum methods. arXiv:1012.6031.